Grand Valley State University
ScholarWorks@GVSU

Peer Reviewed Articles

Chemistry Department

9-2018

Nascent O_2 ($a^1\Delta_g$, v = 0, 1) Rotational Distributions from the Photodissociation of Jet-Cooled O_3 in the Hartley Band

Michelle L. Warter
Texas A & M University - College Station

Carolyn E. Gunthardt
Texas A & M University - College Station, cgunthardt@tamu.edu

Wei Wei
Texas A & M University - College Station

George McBane
Grand Valley State University, mcbaneg@gvsu.edu

Simon W. North
Texas A & M University - College Station, swnorth@tamu.edu

Follow this and additional works at: https://scholarworks.gvsu.edu/chm_articles

Part of the Physical Chemistry Commons

Recommended Citation

Warter, Michelle L.; Gunthardt, Carolyn E.; Wei, Wei; McBane, George; and North, Simon W., "Nascent O_2 ($a^1\Delta_g$, v = 0, 1) Rotational Distributions from the Photodissociation of Jet-Cooled O_3 in the Hartley Band" (2018). *Peer Reviewed Articles*. 42.
https://scholarworks.gvsu.edu/chm_articles/42

This Article is brought to you for free and open access by the Chemistry Department at ScholarWorks@GVSU. It has been accepted for inclusion in Peer Reviewed Articles by an authorized administrator of ScholarWorks@GVSU. For more information, please contact scholarworks@gvsu.edu.

Nascent O_2 ($a\ ^1\Delta_g$, v = 0, 1) Rotational Distributions from the Photodissociation of Jet-Cooled O_3 in the Hartley Band

Michelle L. Warter [a, †], *Carolyn E. Gunthardt* [a, †], *Wei Wei*[a], *George C. McBane*[b], *and Simon W. North*[a,]*

[a]Department of Chemistry, Texas A&M University, College Station, Texas 77842
[b]Department of Chemistry, Grand Valley State University, Allendale, Michigan 49401

[†]Both authors contributed equally to this work

Abstract: We report rotational distributions for the O_2 ($a\ ^1\Delta_g$) fragment from photodissociation of jet-cooled O_3 at 248, 266, and 282 nm. The rotational distributions show a population alternation that favors the even states, as previously reported for a 300 K sample by Valentini et al. (*J. Chem. Phys*. **86**, 6745 (1987)). The alternation from the jet-cooled precursor is much stronger than that observed by Valentini et al., and in contrast to their observations does not depend strongly on O_2 ($a\ ^1\Delta_g$) vibrational state or photolysis wavelength. The odd/even alternation diminishes substantially when the ozone beam temperature is increased from 60 to 200 K, confirming its dependence on parent internal energy. The magnitude of the even/odd alternation in product rotational states from the cold ozone sample, its temperature dependence, and other experimental and theoretical evidence reported since 1987 suggest that the alternation originates from a Λ-doublet propensity, and not from a mass independent curve crossing effect as previously proposed.

Submitted to: *Journal of Chemical Physics* September 10, 2018
8 Figures

proofs to: Simon W. North
Department of Chemistry
Texas A&M University
P.O. Box 30012
College Station, TX 77842
Fax: 979-845-2971
e-mail: swnorth@tamu.edu

Introduction

The photodissociation of ozone in the Huggins-Hartley band plays a critical role in atmospheric processes[1] and has been the subject of numerous theoretical[2-8] and experimental[9-18] studies. Excitation is due to a 1 $^1A'$ ($^1A_1$ in C_{2v}) to 3 $^1A'$ ($^1B_2$ in C_{2v}) transition, called B←X, and results primarily in dissociation into two spin-allowed product channels[8],

$$O_3 + h\nu \rightarrow O_2\,(^3\Sigma_g^-) + O\,(^3P) \qquad (1)$$

$$\rightarrow O_2\,(^1\Delta_g) + O\,(^1D). \qquad (2)$$

Channel 2 is the dominant channel throughout the Hartley band with a quantum yield ranging from 0.83 to 1.00.[19-21] A repulsive state (R) of $^1A'$ symmetry crosses the B state near its shallow well and leads to triplet products. A second excited state (A) of $^1A'$ symmetry, of comparable energy to the B state in the Franck-Condon region, plays only a minor role in the photochemistry.[4] A recent theoretical study has shown that despite the number of possible couplings, the dynamics among the X, A, B, and R states are dominated by initial excitation to the B state followed by either dissociation on the B state (channel 2) or crossing to the R state (channel 1).[3] The preference for diabatic dynamics leading to channel 2 over the adiabatic pathway to the ground state products reflects the small coupling between the B and R states and the large separation speeds in the photodissociation. Classical trajectory calculations using this two-state model have been able to reproduce most of the experimental observations.[3, 5]

O_2 (a $^1\Delta_g$) vibrational and rotational distributions arising from photodissociation in the Hartley band have been previously reported.[3, 13, 14, 22] The vibrational distributions peak at v=0 and monotonically decrease with increasing vibrational quantum number, a result reproduced by theoretical calculations. These results are consistent with dynamics characterized by vibrational adiabaticity.[23] The rotational distributions of O_2 (a $^1\Delta_g$) from a 300 K ozone sample were reported by Valentini and coworkers[14] at wavelengths between 230 and 311 nm. The distributions are approximately Gaussian in shape and peaked at high J (approximately J=35) for 240 nm with the maximum shifting to lower J with increasing wavelength. Trajectory calculations[3] yield rotational distribution envelopes that are qualitatively similar, with some quantitative differences that probably result principally from errors in the angular dependence of the B-state surface.

Valentini et al. also observed that the populations of the odd rotational states were low relative to the even states. This population alternation was largest at 240 nm, and diminished to very small amplitude at wavelengths > 293 nm. The difference between odd and even states decreased with increasing O_2 ($a\ ^1\Delta_g$) vibrational state for every wavelength. No even/odd alternation was observed in O_2 ($a\ ^1\Delta_g$) produced by microwave discharge, implying that in the ozone experiment the alternation resulted from photodissociation dynamics. Valentini et al.[14] considered two candidate explanations for the alternation: a propensity for formation of a particular Λ-doublet state in the $a\ ^1\Delta_g$ product, and a *J*-selective crossing probability to the R state that selectively depleted the odd-*J* levels from the singlet product distribution.

In linear molecules, rotational levels with nonzero orbital angular momentum consist of a pair of states, degenerate in the absence of rotation, referred to as Λ doublets. The wavefunctions of the two Λ doublets have opposite symmetry with respect to reflection through a plane containing the plane of rotation. The wavefunction of the Λ(A′) component is symmetric with respect to reflection, while that of the Λ(A′′) component is antisymmetric with respect to reflection.[24] Due to symmetry restrictions concerning the exchange of two indistinguishable spin-zero nuclei, $^{16}O_2$ ($a\ ^1\Delta_g$) molecules in the Δ(A′) component can have only even rotational states, while molecules in the Δ(A′′) can have only odd rotational states. A propensity for the formation of the Δ(A′) component could therefore lead to the observed odd/even alternation. In ozone dissociation, this propensity has a clear dynamical motivation: in the limiting case of a *J*=0 excited ozone molecule on a $^1A'$ surface, conservation of symmetry would lead to the Δ(A′) Λ-doublet component and therefore to only even *J*.

To motivate the selective-curve-crossing model Valentini et al. argued that since the $^{16}O_2$ ($X\ ^3\Sigma_g^-$) products can have only odd *J* states due to nuclear spin statistics, only the fragmenting ozone molecules evolving toward odd-*J* product states can couple to the R state to give triplet products. (Within their impulsive model of the dissociation it was plausible to assume that the final rotational state of the O_2 product was already established at the time the B/R crossing seam was reached.)

To distinguish between these possibilities they carried out an experiment on an isotopically enriched ozone sample containing equal amounts of ^{16}O and ^{18}O. The results (*vide infra*) led them to recommend the *J*-selective crossing probability as the origin of the alternation.

The selective-crossing interpretation of the alternation has generally been accepted in the dynamics community, though little new evidence in its favor has appeared. A few groups have expressed concerns, especially on theoretical grounds. Baloïtcha and Balint-Kurti[2] recommended alternative approaches based on angular momentum considerations, though they did not present a complete model. Recent symmetry adapted calculations from Picconi and Grebenshchikov[25], intended to model the selective crossing probability mechanism, do not show any odd/even population alternation. New studies on the rotational angular momentum polarization of the O_2 ($a\ ^1\Delta_g$) fragments also provide clues toward the origin of the alternation.[26, 27] In particular, differences in the vector correlations associated with the even and odd states have been observed and persist even at wavelengths where there is no longer a clear population alternation.

State-resolved rotational distributions measured in free-jet expansions have not been reported. Any difference between those distributions and the 300K results would reflect influence of initial parent internal energy on the population alternation. The current paper presents such measurements at 248, 266, and 282 nm. They reveal significantly greater even/odd alternation than observed in the 300 K experiment of Valentini et al.,[14] indicating that parent internal energy plays an important role in the alternation. The strong alternation we observe, together with earlier measurements demonstrating a very weak temperature dependence of the singlet/triplet branching ratio, provide strong evidence that the alternation is unrelated to the B/R crossing probability. Weighing the evidence, we conclude that the observed odd/even alternation originates from a Λ-doublet propensity, and not from a *J*-selective curve crossing effect as previously suggested.

Experimental

The molecular beam/velocity-map ion imaging apparatus has been described in detail previously.[28, 29] A collimated pulsed supersonic molecular beam of ozone was created by flowing helium over O_3 trapped on silica gel beads at ~-55°C for a total pressure of ~800 torr and expanding the beam through a General Valve series 9 pulsed valve. The molecular beam was intersected at 90° by two co-propagating linearly polarized laser beams. The 248 nm dissociation light was produced with a KrF GAM-10 excimer laser, the 266 nm light by frequency doubling the 532 nm output of a Big Sky ULTRA CFR Nd:YAG laser, and the 282 nm light by frequency doubling the output of a dye laser (Quanta-Ray PDL - 1) pumped by a Spectra Physics LAB-150-10 Nd:YAG laser. The probe light was the frequency doubled output of a dye laser (LAS LDL 2051) operating in the range of 604–640 nm, pumped by another Spectra Physics LAB-150-10. Its wavelength was accurately determined by optogalvanic calibration using a Cu-Ne hollow cathode lamp. The O_2 (a $^1\Delta_g$) fragments were probed using 2+1 resonance-enhanced multiphoton ionization (REMPI) using the d $^1\Pi_g$ state, a low-lying Rydberg state that interacts with the nearby II $^1\Pi_g$ valence state.[30-32] This interaction causes the d $^1\Pi_g$ (v' = 1–3) states to predissociate to the O (^{3}P) + O (^{3}P) channel, producing perturbations in the rotational spectra. Although REMPI via these states has been used previously in the study of ozone[9-11] photodissociation, using these states does not provide accurate rotational populations. Vibrational states $v' \geq 4$ are above the dissociation threshold for the II $^1\Pi_g$ state and do not show any effects of perturbation in the rotational distributions.[30] We therefore employed excitation to v' = 4. The resultant O_2 cations were accelerated by velocity mapping electrostatic lenses prior to entering the 50 cm long field-free flight tube coaxial with the molecular beam. The ion clouds were projected onto a position-sensitive microchannel plate phosphor screen assembly gated to detect the mass of interest. A photomultiplier tube (PMT) detected the entire ion signal as the probe laser was scanned to collect the rotational spectrum.

The rotational temperature of the beam could be varied by changing the pulsed valve timing. It is well documented[33] that the rotational temperature in a pulsed free jet varies within the pulse, warmer at early times and coldest near the center of the pulse. The rotational temperature ranged from 60±10 K to 200±20 K as determined using 1+1 REMPI of the A←X transition of NO at 226 nm[34] using the same seed ratio, total stagnation pressure, and pulsed valve timing employed in the photodissociation experiments.

Classical trajectory calculations with surface hopping[35] were carried out as described by McBane et al.[3] for 282 nm photodissociation. They used the potential surfaces and coupling functions for the B and R states described by Schinke and McBane.[4] Trajectories began on the B state with coordinates and momenta selected to model the ground state vibrational wavefunction of ozone, with total angular momentum $J=0$, and with total energy within 0.01 eV of 4.575 eV. After the fragments had separated, the rotational energy E_{rot} of the diatomic product was computed from the final momenta and coordinates, converted to a "classical rotational quantum number" using the rotational constant of $O_2(a)$, and rounded to the nearest integer. Vibrational states were assigned by computing a classical vibrational quantum number from the vibrational energy and the known harmonic frequency and anharmonicity of $O_2(a)$ and rounding to the nearest integer. Product state distributions were then constructed by weighted sums over all trajectories resulting in each (v,j), using weighting factors proportional to the square of the electronic transition dipole moment evaluated at the starting geometry for each trajectory.

Results and Analysis

Rotational distributions were measured for O_2 ($a\ ^1\Delta_g$) fragments following the UV photolysis of ozone. All rotational spectra were obtained by scanning the probe laser and collecting the overall signal with a PMT. The spectra were collected in segments and multiple spectra of each segment were averaged together. The segments were baseline and power corrected before being combined. The final experimental spectra were fit with a simulation using O_2 ($a\ ^1\Delta_g$) diatomic constants calculated by fitting the term values from Morrill et al.[30] using a nonlinear least squares fit. The spectra were fit assuming a Gaussian peak shape and using relative line strength ratios calculated from the two-photon line strength expressions from Bray and Hochstrasser.[36] The fractional line strengths for the S:R:Q:P:O branches are 0.22:0.28:0.01:0.22:0.27 for $J=20$. Modest differences from these calculated values were observed and are attributed to laser power drift and beam overlap. The Q branch is predicted to be weak, especially at high *J*, and is not observed in the experimental spectra.

The overlapping states in the P and O branches were difficult to fit accurately, so the fits relied heavily on the isolated peaks of the R and S branches for the *v*=0 spectra. We observed overlap between the R and S branches in the *v*=1 spectra at all photodissociation wavelengths, reducing the number of isolated peaks. However, the line strength ratios for the S and R branches are well known and this constraint was valuable in fitting the spectra where the branches overlapped. As confirmation of the relative intensities, ion images were collected for these overlapping peaks, and relative contributions from the R and S branches could be quantified by integrating peaks in the derived speed distributions. All the experimental and calculated rotational distributions have been individually normalized for comparison.

To quantify the differences between the even and odd *J* state populations we define a suppression factor, $S(J_{odd})$,

$$S(J_{odd}) = \frac{P(J_{even}) - P(J_{odd})}{P(J_{even})} \quad (3)$$

where $P(J_{odd})$ is the population of a given odd rotational state, and $P(J_{even})$ is the average population of the neighboring even states. A suppression factor of 0 corresponds to no suppression and 1 corresponds to complete suppression of the odd state relative to the adjacent even states.

The experimental rotational spectrum and corresponding simulation for O_2 ($a\ ^1\Delta_g$) *v*=0 from 248 nm dissociation are shown in Figure 1. In this spectrum, the P-, R-, S-, and O-branches are clearly observed. The O branch exhibits a bandhead, while the majority of the peaks in the P-, R- and S-branches are well resolved. The rotational populations for O_2 ($a\ ^1\Delta_g$) *v*=0 derived from the spectrum are shown in Figure 2. Representative error bars shown Figure 2 were determined through a comparison of the rotational distributions derived from independent fits of the P-branch and R-branch regions of the REMPI spectrum. We believe there should be little variation in experimental uncertainty with photolysis wavelength or product vibrational state, and thus these error bars are meant to provide an estimation of the uncertainty for all rotational distributions reported. Classical trajectory results are shown for comparison. To facilitate comparison with the classical trajectory calculations, which do not include electronic orbital angular momentum, the experimental rotational distributions have been plotted in terms of *N*, the angular momentum due to nuclear rotation. *J* values, which include the sum of the orbital and rotational angular momenta, were converted to *N* values by subtracting the 2 quanta of orbital angular momentum associated with the Δ electronic state. The experimental distribution is approximately Gaussian and is peaked at N=30; it is consistent with the rotational reflection principle.[23] The theoretical and experimental results are in excellent agreement, although the calculations do not exhibit a population alternation. In the experimental distribution, the odd state populations are significantly lower than the populations of the neighboring even states. The suppression factors range from 0.74 to 0.96 across the distribution.

The R- and S- branches of the rotational spectrum for O_2 ($a\ {}^1\Delta_g$) v=1 at 248 nm are shown in Figure 3. There is an overlap of several peaks in the R and S-branches, so fewer peaks than expected are observed. The experimental rotational distribution, shown in Figure 4, peaks at N=28, while the trajectory results peak at N=24. The v=1 distribution is broader than v=0 which may be a consequence of overlapping states of the R and S-branches. This overlap complicates extraction of accurate populations, particularly for the lowest rotational states. No decrease in the odd/even alternation is observed in the v=1 distribution compared to the v=0 distribution. The v=1 suppression factors range from 0.77 to 0.95 over the distribution**.** The suppression factors associated with the 300 K measurements of Valentini and co-workers are 0.30 and 0.22 for v=0 and v=1 at the peaks of the respective distributions, significantly lower than we observe. We see no clear evidence that the odd/even alternation decreases with increasing vibrational state, in contrast to the 300 K results.

The v=0 rotational distribution for the 266 nm photolysis of ozone is shown in Figure 5. It peaks near N=20 and the odd/even population alternation is still clearly present in the experimental results. In contrast to the earlier study, the magnitude of the alternation has not diminished significantly from 248 nm; the suppression factors range from 0.75 to 0.92 across the distribution. The overall shape of the distribution is in good agreement with the trajectory results.

The *v*=1 rotational distribution from 266 nm photolysis is shown in Figure 6. The distribution is in qualitative agreement with the trajectory results. Similarly to the 248 nm *v*=1 distribution, the population of the odd *J* states is still strongly suppressed relative to the neighboring even states for *v*=1, corresponding to a suppression factors of 0.75-0.95 across the distribution. The experimental distribution is peaked near *N*=16, while the trajectory results are peaked at 17.

The *v*=0 O_2 ($a\ ^1\Delta_g$) rotational distribution arising from photolysis at 282 nm is shown in Figure 7. The peak of the rotational distribution has shifted to *N*=12. The peaks in the REMPI spectrum consist of unresolved P and O-branch bandheads and overlapping R- and S-branches which makes extraction of the populations difficult. We find that there is too much overlap of the low *J* states ($N \leq 4$) to accurately determine the population of these states, although the best fit values are reported (open circles). There is reasonable agreement with the trajectory results for the higher *N* states. Despite the overlapping transitions a clear population alternation is observable. The suppression factors are still very strong, ranging from 0.65 to 0.90. The odd/even alternation in the 282 nm distribution has not decreased compared to the 248 and 266 nm distribution. In contrast, Valentini and coworkers reported very little alternation in their 293 nm distribution, with some odd state populations that are not suppressed.[14]

Discussion

Comparison of observations

The results described above from photolysis of jet-cooled ozone differ in several ways from the 300 K rotational distributions reported by Valentini and coworkers.[14] The rotational distributions reported in the current paper are shifted to lower *J* states compared to the rotational distributions reported by Valentini and coworkers. This discrepancy can be explained by the difference in parent internal energy for jet-cooled and 300 K samples, as discussed previously by Levene and Valentini.[37] The current results show improved agreement with recent trajectory calculations since the jet-cooled sample provides a better comparison to calculations performed at total parent J=0. The even/odd alternation observed by Valentini *et al.*[14] is strongest at shorter photolysis wavelengths and low O_2 ($a\ ^1\Delta_g$) vibrational states. For example, little alternation is observed at the longest wavelength (293 nm) studied. In contrast to those measurements, our results from cold ozone show a stronger alternation that does not significantly change with either photolysis wavelength or O_2 ($a\ ^1\Delta_g$) vibrational state.

Triplet yield

The B/R curve crossing is the only significant pathway to triplet products. Thus, if the crossing is responsible for depletion of the odd states from the O_2 ($a\ ^1\Delta_g$) rotational population then the difference between the even and odd J state population should provide a measure of the quantum yield for channel 1. On this basis, Valentini et al. calculated the triplet yield using

$$\Phi_1 = \frac{\sum_{J_{even}} P(J_{even}) - \sum_{J_{odd}} P(J_{odd})}{2\sum_{J_{even}} P(J_{even})}, \qquad (4)$$

where the populations for the even and odd states were summed over all vibrational states and weighted by the vibrational branching ratios. This approach results in triplet yields of ϕ_1=0 for no suppression (S=0) and approximately ϕ_1=0.5 in the case of zero odd state population (S=1).

The J-selective curve crossing model implies that the increased alternation observed under jet-cooled conditions corresponds to an increase in the triplet channel quantum yield. Sparks et al.[38] studied the photodissociation of jet-cooled ozone at 266 nm using photofragment translational spectroscopy (PTS), and Huber and coworkers[13] reported a similar experiment at 248 nm. Both groups obtained triplet yields of ϕ_1=0.1. For comparison to those measurements, we have used the analysis of Valentini et al.[14] (equation 4) to estimate the triplet quantum yield using suppression factors measured in the present study. We did not measure rotational distributions for every populated O_2 ($a\ ^1\Delta_g$) vibrational state, but v=0 and v=1 products account for 64% and 80% of the population for 248 and 266 nm, respectively[13, 22], and near 280 nm the v=0 products account for over 70% of the vibrational population. We therefore determined best estimates and lower and upper bounds for the quantum yields based on different assumptions

AIP Publishing

about the alternation in the unobserved states. The best estimate was computed assuming the rotational distributions for the unobserved vibrational states (*v*>1 for 248 and 266 nm, and *v*>0 for 282 nm) had the same average suppression as the observed state(s). The lower bound was calculated assuming the distributions for the unobserved states had no suppression (S=0) and therefore no contribution to the triplet yield, while the upper limit was determined assuming the rotational distribution for the unobserved states had total suppression (S=1) and contributed 50% to the triplet channel. Using this model, the calculated quantum yields for the triplet channel are $\phi_1=0.41^{+0.04}_{-0.10}$ at 248 nm, $\phi_1=0.41^{+0.03}_{-0.06}$ at 266 nm, and $\phi_1=0.40^{+0.03}_{-0.09}$ at 282 nm. The triplet yields at 248 and 266 nm assuming the J-selective curve crossing model are significantly greater than the 0.1 obtained in the previous jet-cooled measurements.

We know of no independent measurement of the triplet yield from jet-cooled ozone at 282 nm or longer wavelengths, but relevant data are available from cooled bulk samples. Talukdar et al. reported[39] that the O(^{1}D) quantum yield was 0.89±0.02, corresponding to a triplet yield of 0.11, independent of wavelength between 289 and 305 nm and independent of temperature in the range 203–320K. The NASA/JPL recommended quantum yield for the triplet channel over the entire range 220–305 nm is 0.10, independent of temperature.[17, 21, 39-41] These values are significantly smaller than the $\phi_1=0.40^{+0.03}_{-0.09}$ we obtain from our measurements at 282 nm on the basis of the curve-crossing model.

Parent internal energy dependence

The maximum suppression factor of the 300 K rotational distributions is 0.63 for *v*=0 at 240 nm, which is smaller than any of the suppression factors in the jet-cooled experiment. In comparison, the present results show a maximum suppression factor of 0.96. This difference in the suppression factors suggests that the degree of odd/even alternation is a function of parent internal energy. To examine the temperature dependence of the alternation, we measured O_2 ($a\ ^1\Delta_g$) rotational REMPI spectra following photodissociation at 266 nm at two different positions in the pulsed beam, yielding beam temperatures of 60 ± 10 K and 200 ± 20 K. The (2, 0) probe transition was selected because the intensity alternation is not as strong in the (2, 0) band as the

(4, 0) band, allowing minor changes in the alternation to be detected more easily. While quantitative rotational populations and suppression factors cannot be obtained from the (2, 0) band, qualitative changes in the strength of odd/even population alternation can be clearly observed with changing beam temperature. Spectra of the (2, 0) band were obtained for each temperature and the 60 and 200 K spectra are shown in Fig. 8. Increasing the beam temperature, and hence the parent internal energy, resulted in an increased odd *J* state population, diminishing the intensity alternation. In the 60 K spectrum, strong population alternation is present, with the intensity of each even peak greater than its neighboring odd state(s). In the 200 K spectrum, however, no alternation is present and the intensity smoothly decreases with decreasing *J*. The use of the (2, 0) band allows for direct comparison with a previous study, as Hancock et al used the same REMPI band to probe the photoproducts of ozone dissociation in a 140 K beam.[42] Spectra were measured using 270 nm and 300 nm photolysis wavelengths, and the authors noted the presence of odd/even alternation in the R and S branches at 270 nm. The degree of alternation from their study is intermediate between the 60 and 200 K spectra shown in Figure 8. The four observations near 266 nm at different temperatures – ours at 60 and 200 K, that of Hancock et al. at 140 K, and that of Valentini et al. at 300 K – indicate that the alternation depth decreases with increasing temperature.

It is not clear where a parent-energy dependence would arise in the curve-crossing model, but this dependence arises naturally for the Λ doublet propensity model. The electronic wavefunction of the parent ozone molecule is symmetric with respect to the plane of the molecule. In the case of a planar dissociation (no parent out-of-plane rotation) from a $^1A'$ electronic state, symmetry conservation mandates the exclusive formation of O_2 ($a\ ^1\Delta_g$) in the Δ(A′) doublet. Therefore, in the limit of zero parent internal energy, only fragments in even rotational states can be formed. Relaxation of the symmetry constraints for ozone molecules with nonzero total angular momentum would allow the odd *J* state population to increase. For parent $J \neq 0$, out of plane rotation about the a or b axes would cause a mixing of the Λ doublets and a relaxation of this constraint, leading to formation of odd states. At 300 K the most probable rotational states for the a and b axes are 5 and 15, respectively. In comparison, at 60 K the most probable rotational states for the a and b axes decrease to 2 and 7, respectively. Consequently, a greater degree of Λ doublet mixing is expected at 300 K, resulting in an increase in the relative odd state population. This effect would lead to changes in the odd/even alternation without changing the singlet/triplet branching ratio.

A similar effect has been noted in the photodissociation of H_2O studied by Andresen and coworkers.[43] In this case a strong propensity for the Π(A′′) doublet arising from dissociation in the B state is predicted and observed for a jet-cooled sample. In a thermal sample Andresen and coworkers observed a lack of Λ-doublet propensity as a result of mixing.

Hancock, Horrocks, and coworkers have measured vector correlations in ozone photodissociation to examine this effect.[9-11, 42] They found that for dissociation wavelengths greater than 265 nm, the **v-j** correlation of the odd states was more depolarized than the **v-j** correlation of the even products. The authors attribute this **v-j** alternation to different formation pathways of the two Λ-doublets. The difference in **v-j** correlation between odd and even states shows a strong dependence on radial velocity, increasing for longer photolysis wavelengths and higher *J* fragments. These observations can be explained by the Λ-doublet propensity model. Odd rotational states can only be formed from parent molecules with out-of-plane rotation, and this out-of-plane rotation depolarizes the **v-j** correlation. We note that depolarization due to parent velocity will also serve to depolarize the fragments at low fragment recoil velocities. We are currently reexamining the vector correlations using ion imaging techniques and the results will be the subject of a future study.

Vibrational level dependence

The selective curve crossing model also appears inconsistent with some developments in the theory of ozone photodissociation. Schinke and coworkers[3, 5, 44] studied the coordinate dependence of the B/R coupling strength and developed surface-hopping models of the B/R surface crossing. The crossing probability from B to R can be approximated with a Landau-Zener expression

AIP Publishing

$$P_{cross} = 1 - e^{\left(\frac{-2\pi V_{12}^2}{\hbar v|\Delta F|}\right)}, \qquad (5)$$

where V_{12} is the potential coupling of the B and R states, ΔF is the difference in slopes of the potentials at the crossing point, and v is the radial velocity. The coupling V_{12} tends to increase with the length of the surviving O-O bond at the moment the departing atom reaches the B/R crossing seam. In addition, as that surviving bond length increases, more energy is taken up as potential energy at the crossing so that the crossing speed v decreases, and the slope difference ΔF also decreases. All these dependences combine to make Equation 5 predict that the crossing probability should increase with increasing O-O bond length at the crossing. Since a stretched O-O bond at the crossing seam corresponds to increasing vibrational excitation in product O_2 ($a\ ^1\Delta_g$), the higher vibrational states of the singlet product should be more susceptible to depletion by the crossing to R and should show stronger even/odd alternation according to the selective-crossing model. This tendency of the triplet crossing to deplete the higher vibrational states of the singlet state distribution was recognized by McBane et al.[3] and Qu et al.[5, 44]. Its importance for interpreting the odd/even alternation was stated clearly by Picconi and Grebenshchikov[25], who write "Should the [crossing to triplet] be indeed responsible for the observed depletion of the odd *j* states, one would expect the effect to be the strongest for the highly vibrationally excited O_2 fragments." In the current study, we do not observe a strong dependence of the suppression factors on O_2 ($a\ ^1\Delta_g$) vibrational state, and Valentini et al. observed in their room-temperature experiment that the alternation decreased with increasing vibrational state.

Wavepacket calculations

Picconi and Grebenshchikov[25] performed quantum mechanical dynamics calculations that included identical-nuclei symmetry restrictions in the wavefunctions and a realistic treatment of the coupling between the B and R states. No alternation was present in their results. The authors noted that the crossing seam is located near the bottom of the B state well. At this point, the resulting O_2 ($X\ ^3\Sigma_g^-$) fragment does not have a well-defined rotational state and there is no symmetry-based prohibition against formation of triplet for particular molecules. Beyond the crossing region the O_2 ($a\ ^1\Delta_g$) fragment angular momentum continues to evolve. They state "… the odd *J′* states in R can form from both even or odd *J* states in B."

Isotope experiment

Valentini et al. carried out an isotope enrichment experiment to distinguish between the selective curve crossing and Λ-doublet propensity mechanisms. They prepared ozone from oxygen feedstock containing equal amounts of $^{16}O_2$ and $^{18}O_2$, and stated "CARS spectroscopy of this isotopically mixed ozone showed that it contained all possible O_3 isotopomers, in the statistically expected amounts." They carried out a 266 nm photodissociation experiment using this enriched ozone.

The $^{16}O^{18}O$ molecules (abbreviated '68', following Schinke and coworkers) are not subject to the symmetry restrictions for indistinguishable nuclei, so both even and odd rotational states can appear in the $^3\Sigma^-$ ground state and in both Δ(A′) and Δ(A′′) components of the $^1\Delta$ excited state. Neither candidate mechanism predicts that even/odd alternation will appear in the rotational distribution of the singlet 68 products. In the selective curve crossing model, even and odd rotational states should be equally depleted by curve crossing, and the triplet yield of 68 should be twice that seen for 66 products. In the Λ doublet propensity model, the propensity would still be present but no enhancement of even rotational levels would result, and the triplet yield should be nearly the same for 68 and 66. Valentini et al. measured the relative populations of the 66 and 68 fragments produced in the mixed isotope, 266 nm photodissociation experiment, dividing the 68 populations by two to adjust for their greater likelihood from a statistical ozone isotopomer distribution. No even/odd alternation was found in the 68 product, as expected. The total adjusted 68 population in the $^1\Delta$ state was only about 75% of the corresponding 66 population and roughly matched the odd-*J* 66 population. Valentini et al. concluded that the triplet yield had in fact increased, and therefore ruled in favor of the curve-crossing model.

To our knowledge, no confirmation of an enhanced triplet yield for 68 product has appeared. The 2012 quantum-mechanical study of Ndengué et al. predicted the triplet branching ratio to be approximately 10 percent regardless of parent ozone isotopomer.[45] Ozone isotope distributions in the stratosphere get transferred to CO_2 through reaction with the $O(^1D)$ ozone photolysis product, and the atmospheric chemistry community studying this effect has not needed to adopt isotopomer-dependent triplet yields for their description.[46] Nonetheless, if the selective curve crossing model is to be discarded, a plausible candidate for the origin of the depletion in 68 product observed by Valentini et al. is needed.

The apparent 68 population shortfall could arise from nonstatistical behavior in the formation and photodissociation of the different ozone isotopomers. A direct comparison between the populations of the 66 and 68 products relies on the assumptions that there is a statistical mixture of O_3 isotopomers and the production of a 68 fragment is twice as likely as the production of a 66 fragment. It is known that the recombination reactions that form ozone are biased in favor of asymmetric isomers (668 rather than 686, for example), up to a few tens of percent at low pressure.[47] If the 300 K sample was in fact depleted in the symmetric isomers 686 and 868 in favor of the asymmetric isomers 668 and 688, then one would expect to see less 68 product than the pure statistical expectation because the middle atom cannot be ejected in normal ozone photodissociation. Such a nonstatistical ozone isotopomer distribution should have been detectable in the CARS control experiment, though it is not clear whether the CARS vibrational band strengths and intensities were well enough known to rule it out. In addition, there could be dynamical preferences in which bond breaks in the photodissociation of asymmetric ozone isotopomers, or isotope selectivity in the curve-crossing probability arising from origins other than nuclear spin statistics. A theoretical study by Ndengué et al.[45] concluded that for the photodissociation of the 668 isotopomer in the Hartley band, there was a slight preference for the formation of the 68 diatomic fragment. This preference was attributed to a kinetic effect resulting in the preferential ejection of the lighter atom and to an asymmetry in the ground state wavefunction. While these calculations did not include the 886 isotopomer due to its low natural abundance, it is likely that a similar effect in the photodissociation of this isotopomer could lead to preferential formation of the 88 diatom, at the expense of 68. These dynamical preferences suggest that the ratio of the probabilities of forming the 68 and 66 photofragments from a statistical mixture of O_3 isotopomers may deviate from the statistical prediction of 2:1, though the overall effect on the 68 yield is likely to be small. Finally, the curve crossing probability is not necessarily mass-independent. The curve crossing probability depends strongly on the length of the surviving bond at the moment the departing atom passes the crossing seam.[3] The longer the surviving bond, the more likely there will be a crossing to the triplet surface. Since the dynamics of the dissociation will depend on the masses of the atoms, the distribution of surviving bond lengths will be different for each isotopomer. The study by Ndengué et al. indicates this effect is real but again small.

Conclusion

In our view the weight of the evidence justifies adopting the Λ-doublet propensity model to interpret the observed even/odd alternation. That model has a clear physical origin that is consistent with current theoretical understanding of the dissociation dynamics. The very strong even/odd alternation observed in the jet-cooled experiment would imply an unrealistically large triplet yield within the selective-crossing model. The apparent dependence of the alternation on ozone temperature has a straightforward interpretation within the Λ-doublet propensity model. The vibrational dependence of the alternation observed in the 300 K experiment is opposite that expected from the selective-crossing model together with the current understanding of dynamics at the B/R curve crossing.

Against these arguments for the Λ-doublet propensity model must be set the original isotope experiment of Valentini et al. that led them to select the curve-crossing model instead. They found that the amount of $^{16}O^{18}O$ product from photodissociation of an ozone sample containing equal amounts of the two oxygen isotopes essentially matched the population of the odd-*J* states of $^{16}O^{16}O$, rather than the average of the odd and even populations as would be expected from the Λ-doublet propensity model. We have described a few candidate sources of the suppression, but it is not clear they are the correct ones. Further investigation, and in particular careful measurements of triplet yields from different ozone isotopomers, could help resolve this question. Ion imaging experiments are currently underway to study the vector correlations of the even and odd *J* states to provide more evidence on the origin of the population alternation.

Acknowledgements

The authors would like to thank Victoria Peckham and Colin Wallace for experimental assistance. Support for this project was provided by the Robert A. Welch Foundation (A-1405).

References

1. H. S. Johnston, Annual Review of Physical Chemistry **43**, 1 (1992).
2. E. Baloïtcha and G. G. Balint-Kurti, The Journal of Chemical Physics **123**, 014306 (2005).
3. G. C. McBane, L. T. Nguyen and R. Schinke, The Journal of Chemical Physics **133**, 144312 (2010).
4. R. Schinke and G. C. McBane, The Journal of Chemical Physics **132**, 044305 (2010).
5. Z.-W. Qu, H. Zhu, S. Y. Grebenshchikov and R. Schinke, The Journal of Chemical Physics **123**, 074305 (2005).
6. M.-Y. ZHAO, K.-L. HAN, G.-Z. HE and J. Z. H. ZHANG, Journal of Theoretical and Computational Chemistry **03**, 443 (2004).
7. C. Leforestier, F. LeQuéré, K. Yamashita and K. Morokuma, The Journal of Chemical Physics **101**, 3806 (1994).
8. S. Y. Grebenshchikov, Z. W. Qu, H. Zhu and R. Schinke, Phys Chem Chem Phys **9**, 2044 (2007).
9. G. Hancock, G. A. D. Ritchie and T. R. Sharples, Molecular Physics **111**, 2012 (2013).
10. S. J. Horrocks, G. A. D. Ritchie and T. R. Sharples, The Journal of Chemical Physics **126**, 044308 (2007).
11. S. J. Horrocks, G. A. Ritchie and T. R. Sharples, J Chem Phys **127**, 114308 (2007).
12. R. L. Miller, A. G. Suits, P. L. Houston, R. Toumi, J. A. Mack and A. M. Wodtke, Science **265**, 1831 (1994).
13. M. A. Thelen, T. Gejo, J. A. Harrison and J. R. Huber, The Journal of Chemical Physics **103**, 7946 (1995).
14. J. J. Valentini, D. P. Gerrity, D. L. Phillips, J. C. Nieh and K. D. Tabor, The Journal of Chemical Physics **86**, 6745 (1987).
15. W. Denzer, S. J. Horrocks, P. J. Pearson and G. A. D. Ritchie, Physical Chemistry Chemical Physics **8**, 1954 (2006).
16. D. Stranges, X. Yang, J. D. Chesko and A. G. Suits, The Journal of Chemical Physics **102**, 6067 (1995).

17. Y. Matsumi and M. Kawasaki, Chemical Reviews **103**, 4767 (2003).
18. M. Brouard, A. Goman, S. J. Horrocks, A. J. Johnsen, F. Quadrini and W. H. Yuen, J Chem Phys **127**, 144304 (2007).
19. P. H. Wine and A. R. Ravishankara, Chemical Physics **69**, 365 (1982).
20. A. A. Turnipseed, G. L. Vaghjiani, T. Gierczak, J. E. Thompson and A. R. Ravishankara, The Journal of Chemical Physics **95**, 3244 (1991).
21. K. Takahashi, S. Hayashi, Y. Matsumi, N. Taniguchi and S. Hayashida, Journal of Geophysical Research: Atmospheres **107**, ACH 11 (2002).
22. S. M. Dylewski, J. D. Geiser and P. L. Houston, The Journal of Chemical Physics **115**, 7460 (2001).
23. R. Schinke, *Photodissociation Dynamics*. (Cambridge University Press, Cambridge, 1993).
24. M. H. Alexander, P. Andresen, R. Bacis, R. Bersohn, F. J. Comes, P. J. Dagdigian, R. N. Dixon, R. W. Field, G. W. Flynn, K. H. Gericke, E. R. Grant, B. J. Howard, J. R. Huber, D. S. King, J. L. Kinsey, K. Kleinermanns, K. Kuchitsu, A. C. Luntz, A. J. McCaffery, B. Pouilly, H. Reisler, S. Rosenwaks, E. W. Rothe, M. Shapiro, J. P. Simons, R. Vasudev, J. R. Wiesenfeld, C. Wittig and R. N. Zare, The Journal of Chemical Physics **89**, 1749 (1988).
25. D. Picconi and S. Y. Grebenshchikov, The Journal of Chemical Physics **141**, 074311 (2014).
26. G. Hancock, G. A. D. Ritchie and T. R. Sharples, Molecular Physics **111**, 2012 (2013).
27. S. J. Horrocks, G. A. Ritchie and T. R. Sharples, The Journal of Chemical Physics **127**, 114308 (2007).
28. M. P. Grubb, M. L. Warter, K. M. Johnson and S. W. North, The Journal of Physical Chemistry A **115**, 3218 (2011).
29. H. Kim, K. S. Dooley, E. R. Johnson and S. W. North, Review of Scientific Instruments **76**, 124101 (2005).
30. J. S. Morrill, M. L. Ginter, E. S. Hwang, T. G. Slanger, R. A. Copeland, B. R. Lewis and S. T. Gibson, Journal of Molecular Spectroscopy **219**, 200 (2003).
31. J. S. Morrill, M. L. Ginter, B. R. Lewis and S. T. Gibson, The Journal of Chemical Physics **111**, 173 (1999).
32. W. J. v. d. Zande, W. Koot, J. Los and J. R. Peterson, The Journal of Chemical Physics **89**, 6758 (1988).
33. G. Scoles, D. Bassi, U. Buck, and D.C. Laine (ed.), *Atomic and Molecular Beam Methods*. (University Press, New York, 1988).
34. J. Luque and D. R. Crosley, in *LIFBASE: Database and Spectral Simulation Program* (SRI International Report MP 99-009, 1999).
35. J. C. Tully, The Journal of Chemical Physics **93**, 1061 (1990).
36. R. G. Bray and R. M. Hochstrasser, Molecular Physics **31**, 1199 (1976).
37. H. B. Levene and J. J. Valentini, The Journal of Chemical Physics **87**, 2594 (1987).
38. R. K. Sparks, L. R. Carlson, K. Shobatake, M. L. Kowalczyk and Y. T. Lee, The Journal of Chemical Physics **72**, 1401 (1980).
39. R. K. Talukdar, M. K. Gilles, F. Battin-Leclerc, A. R. Ravishankara, J.-M. Fracheboud, J. J. Orlando and G. S. Tyndall, Geophysical Research Letters **24**, 1091 (1997).

40. J. B. Burkholder, S. P. Sander, J. P. D. Abbat, J. R. Barker, R. E. Huie, C. E. Kolb, M. J. Kurylo, V. L. Orkin, D. M. Wilmouth and P. H. Wine, edited by NASA (2015), Vol. JPL Publication 15-10.
41. R. K. Talukdar, C. A. Longfellow, M. K. Gilles and A. R. Ravishankara, Geophysical Research Letters **25**, 143 (1998).
42. G. Hancock, S. J. Horrocks, P. J. Pearson, G. A. Ritchie and D. F. Tibbetts, J Chem Phys **122**, 244321 (2005).
43. P. Andresen, G. S. Ondrey, B. Titze and E. W. Rothe, The Journal of Chemical Physics **80**, 2548 (1984).
44. Z.-W. Qu, H. Zhu, S. Y. Grebenshchikov and R. Schinke, The Journal of Chemical Physics **122**, 191102 (2005).
45. S. A. Ndengué, R. Schinke, F. Gatti, H.-D. Meyer and R. Jost, The Journal of Physical Chemistry A **116**, 12271 (2012).
46. A. A. Wiegel, A. S. Cole, K. J. Hoag, E. L. Atlas, S. M. Schauffler and K. A. Boering, Proceedings of the National Academy of Sciences **110**, 17680 (2013).
47. R. Schinke, S. Y. Grebenshchikov, M. V. Ivanov and P. Fleurat-Lessard, Annual Review of Physical Chemistry **57**, 625 (2006).

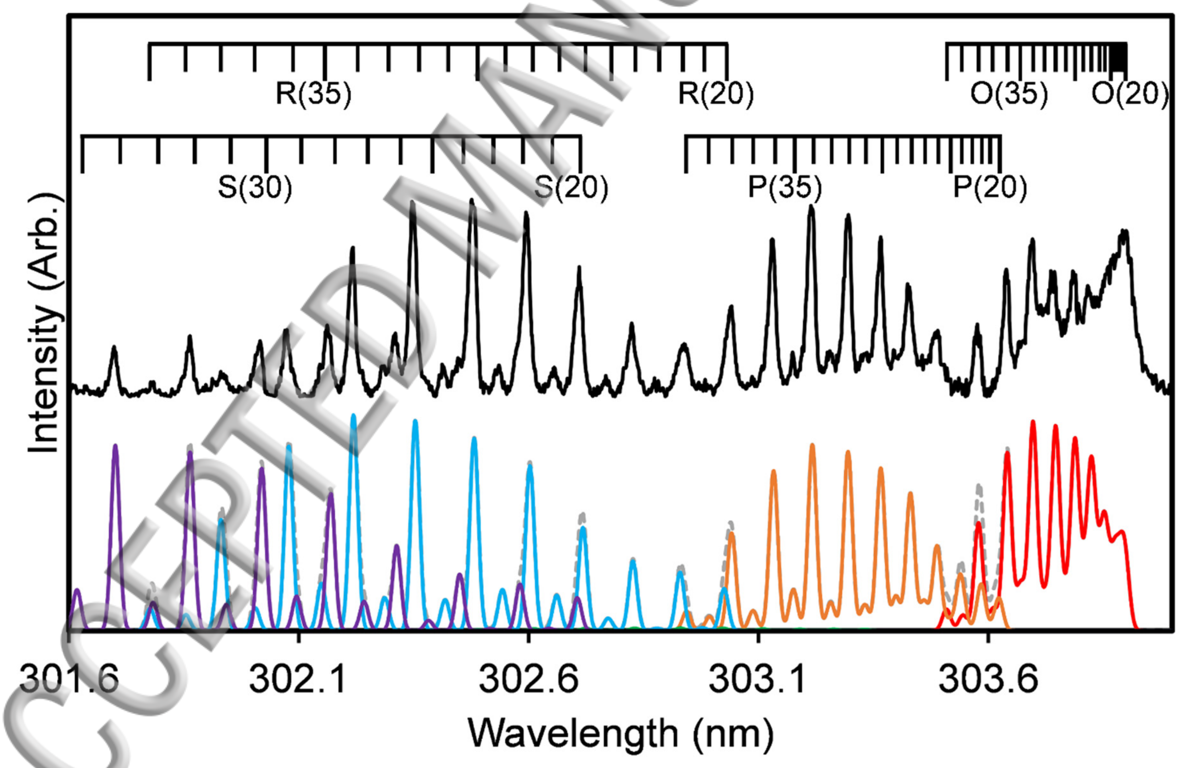

Figure 1. REMPI spectrum of O_2 ($a\ ^1\Delta_g$, v=0) following the photolysis of ozone at 248 nm via the O_2 ($d\ ^1\Pi_g$, v=4) ←← O_2 ($a\ ^1\Delta_g$, v=0) transition. The experimental data (top, black) are compared to the

simulation (bottom). The O (red), P (orange), R (blue), and S (purple) branches are shown with the sum of the branches (gray).

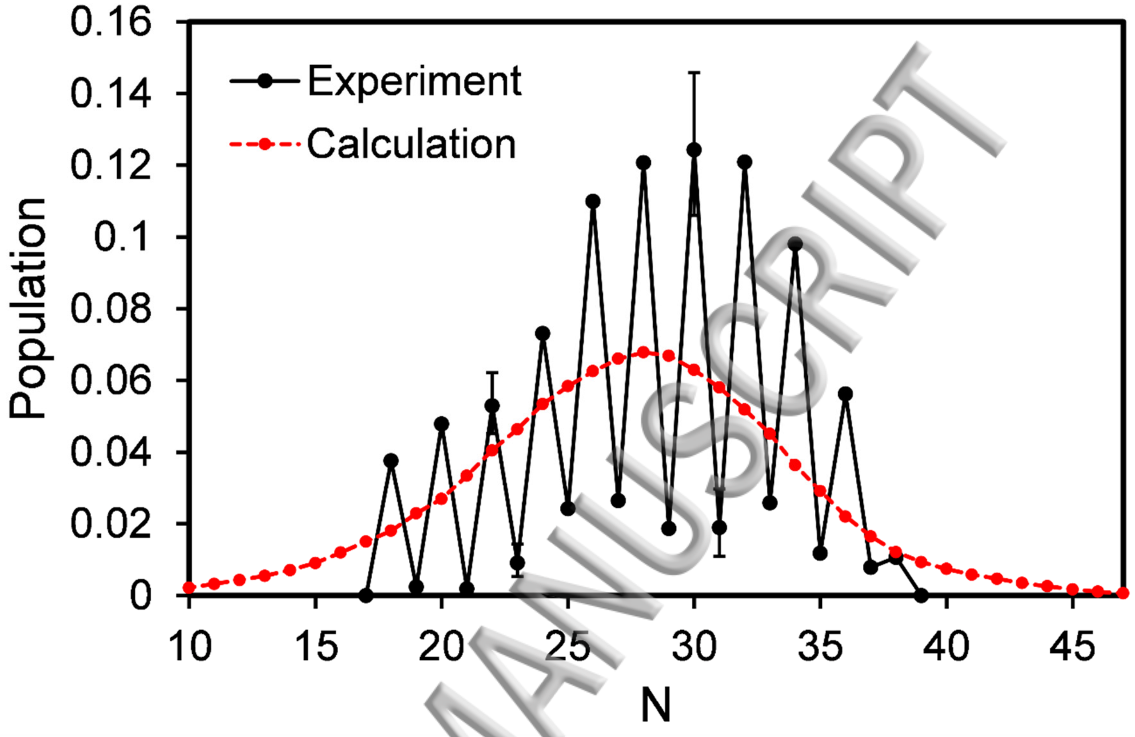

Figure 2. Rotational distributions for O_2 ($a\ ^1\Delta_g$, v=0) following the photolysis of ozone at 248 nm. The experimental results (circles) are compared to the results reported by McBane et al. in ref. 3 (dashed line). Experimental *J* values have been converted to *N* values to facilitate comparison with the classical trajectory calculations (see text for details).

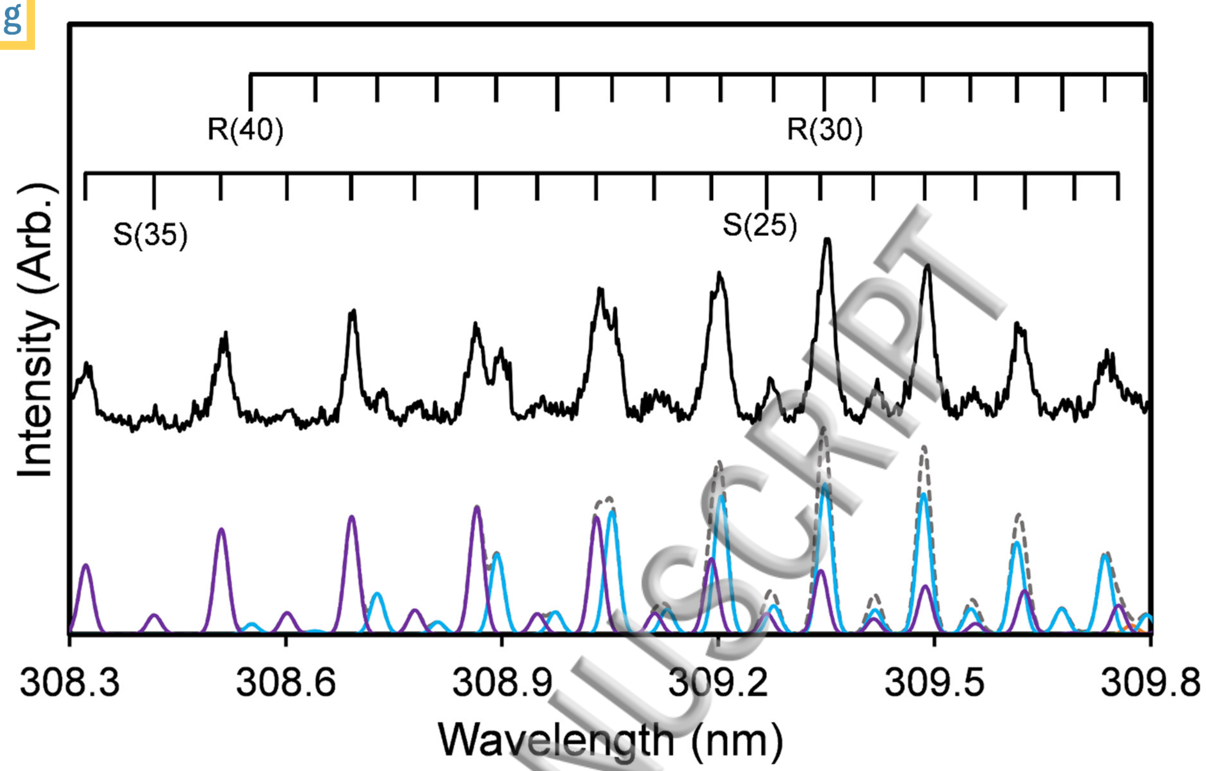

Figure 3. REMPI spectrum of O_2 (a $^1\Delta_g$, v=1) following the photolysis of ozone at 248 nm via the O_2 (d $^1\Pi_g$, v=4) ←← O_2 (a $^1\Delta_g$, v=1) transition. The experimental data (top, black) are compared to the simulation (bottom). The R (blue) and S (purple) branches are shown with the sum of the branches (gray).

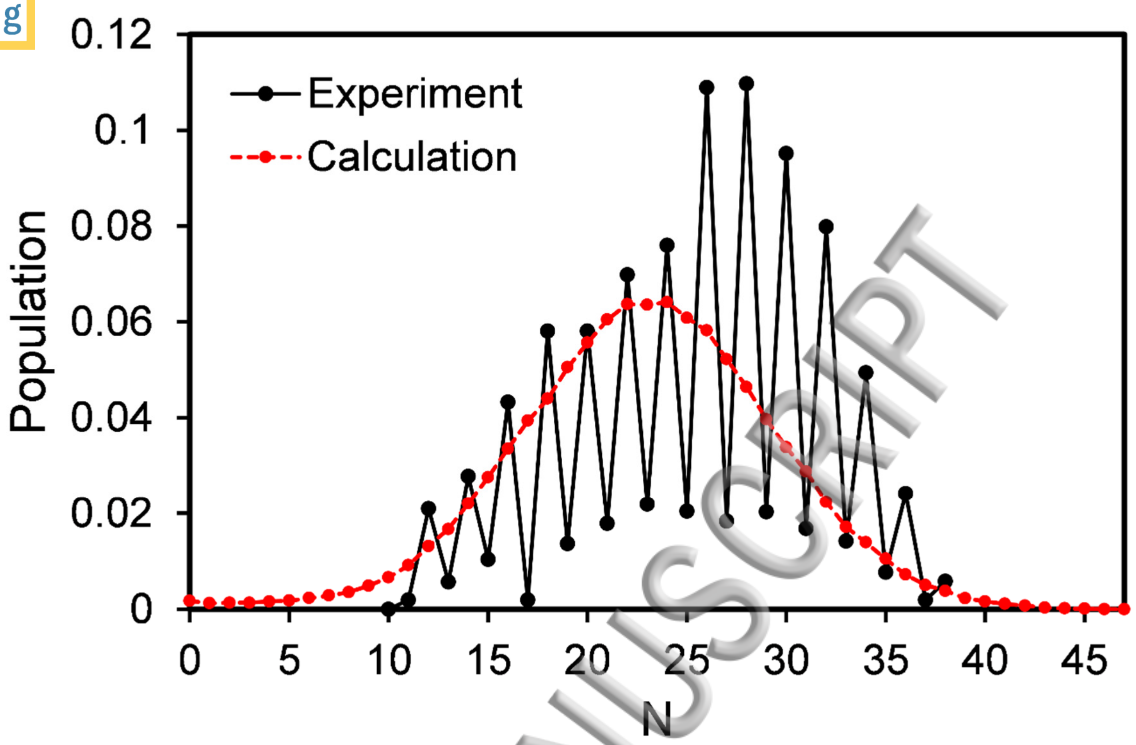

Figure 4. Rotational distributions for O_2 ($a\ ^1\Delta_g$, v=1) following the photolysis of ozone at 248 nm. The experimental results (circles) are compared to the results reported by McBane et al. in ref. 3 (dashed line). Experimental *J* values have been converted to *N* values to facilitate comparison with the classical trajectory calculations (see text for details).

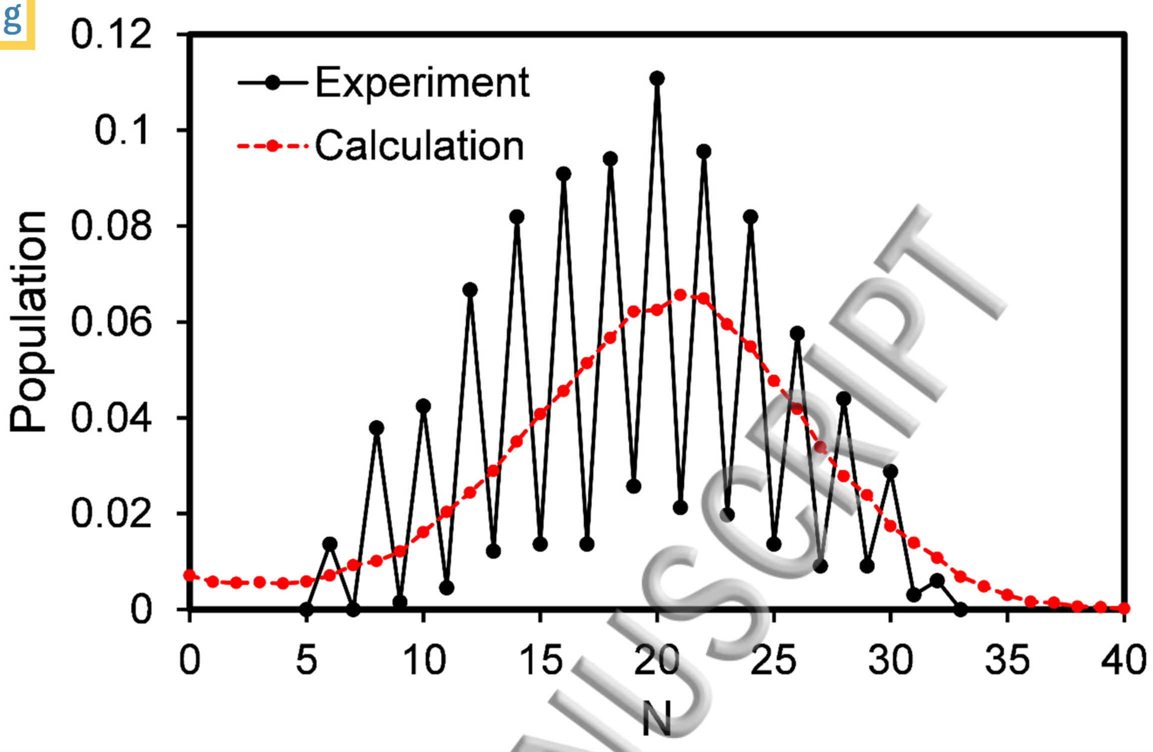

Figure 5. Rotational distributions for O_2 (a $^1\Delta_g$, v=0) following the photolysis of ozone at 266 nm. The experimental results (circles) are compared to the results reported by McBane et al. in ref. 3 (dashed line). Experimental *J* values have been converted to *N* values to facilitate comparison with the classical trajectory calculations (see text for details).

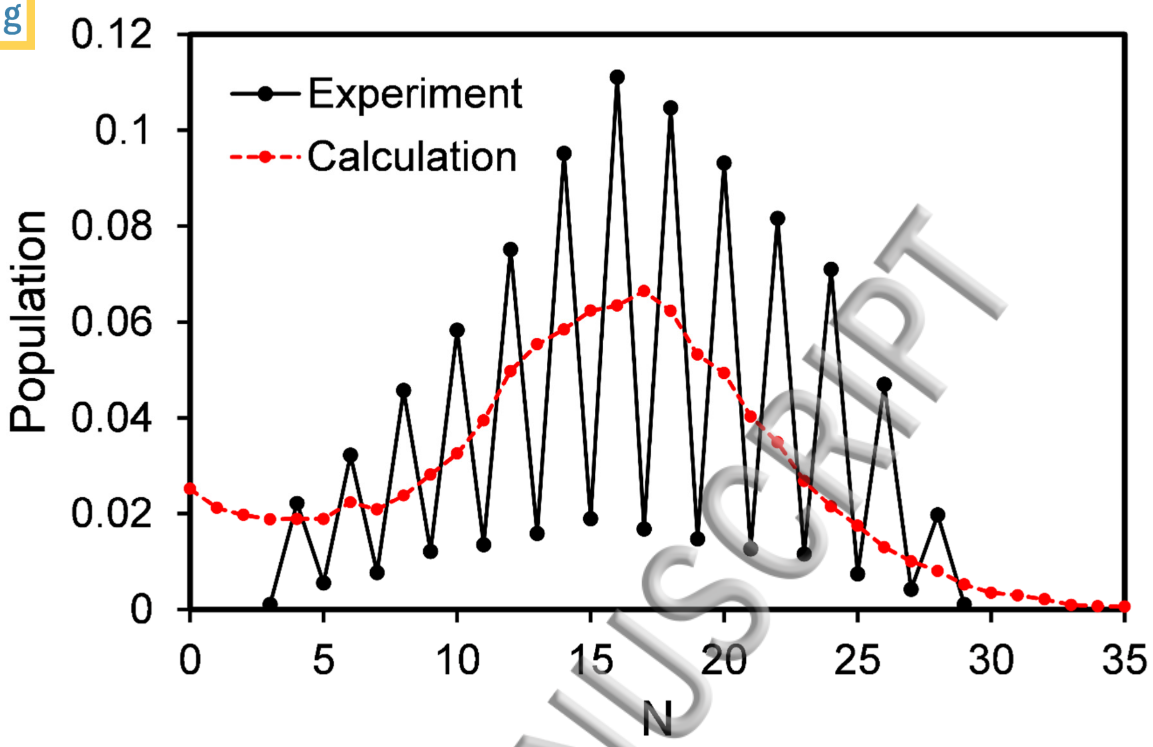

Figure 6. Rotational distributions for O_2 (*a* $^1\Delta_g$, *v*=1) following the photolysis of ozone at 266 nm. The experimental results (circles) are compared to the results reported by McBane et al. in ref. 3 (dashed line). Experimental *J* values have been converted to *N* values to facilitate comparison with the classical trajectory calculations (see text for details).

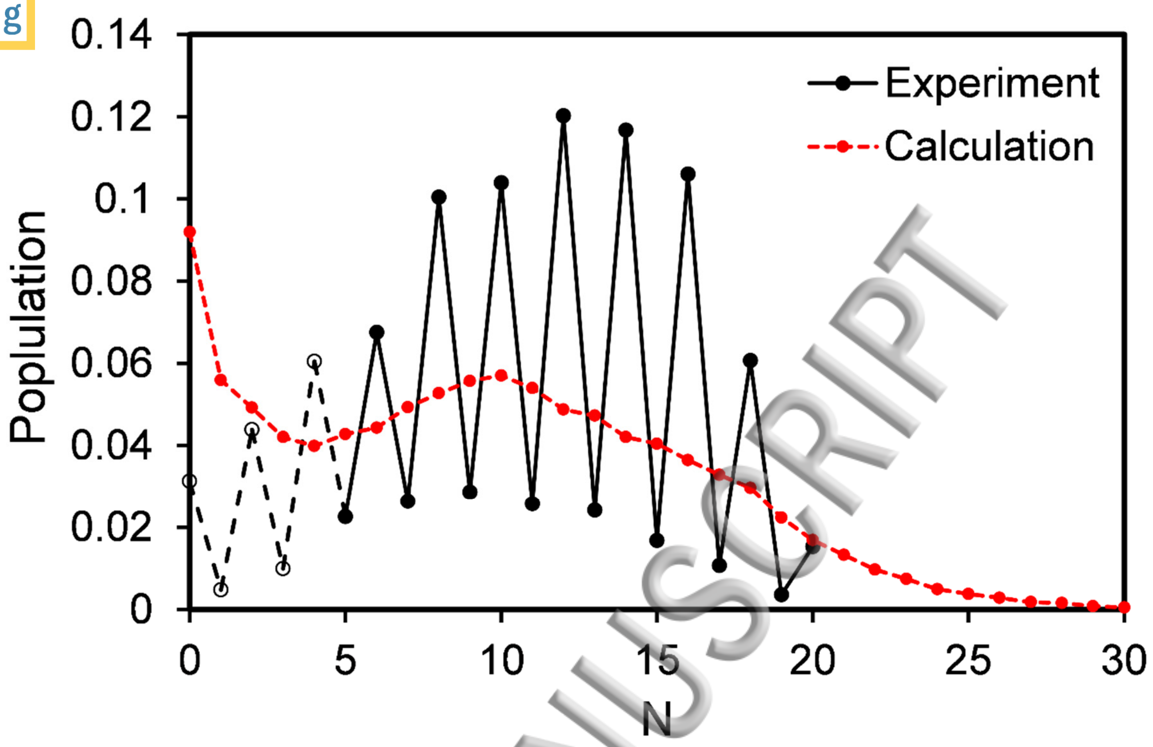

Figure 7. Rotational distribution for O_2 ($a\ ^1\Delta_g$, v=0) following the photolysis of ozone at 282 nm. The experimental data is shown with circles and the open circles indicate the states that could not be accurately fit. The experimental results are compared to the surface-hopping trajectory results (dashed line). Experimental *J* values have been converted to *N* values to facilitate comparison with the classical trajectory calculations (see text for details).

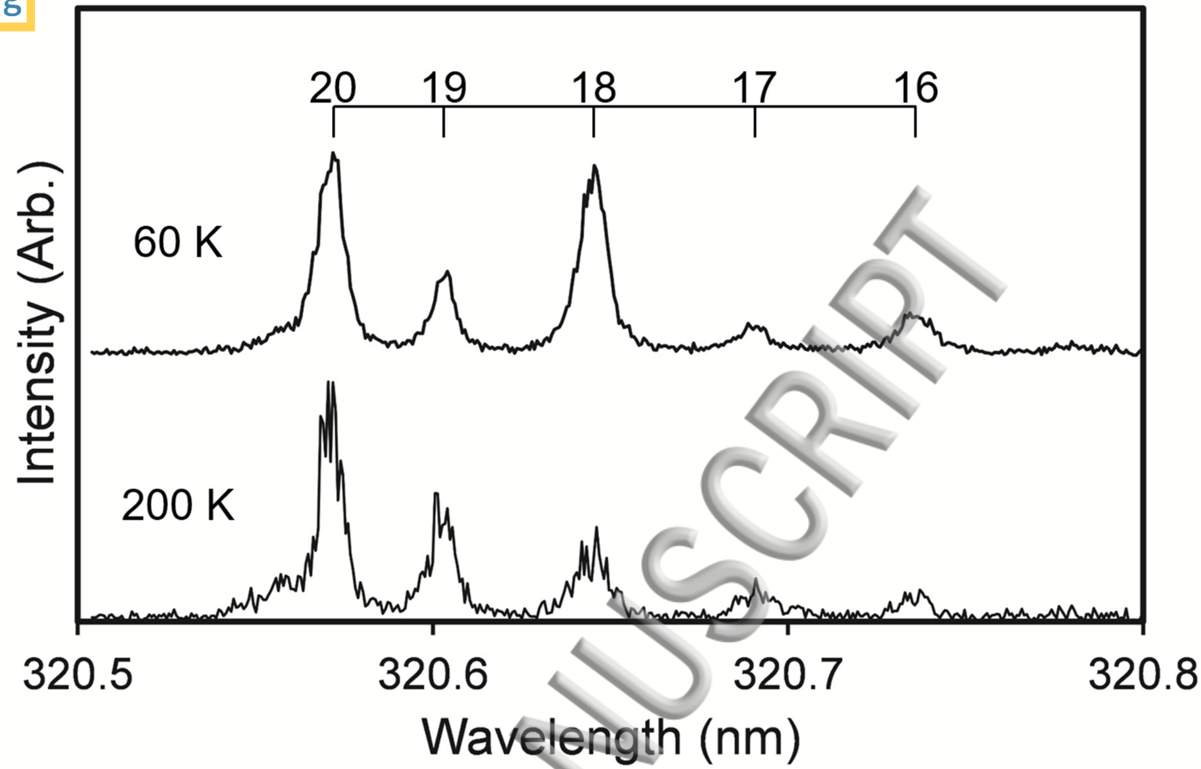

Figure 8. REMPI spectra of O_2 (a $^1\Delta_g$, v=0) following the 266 nm photolysis of ozone via the O_2 (d $^1\Pi_g$, v=2) ←← O_2 (a $^1\Delta_g$, v=0) transition for two beam temperatures.

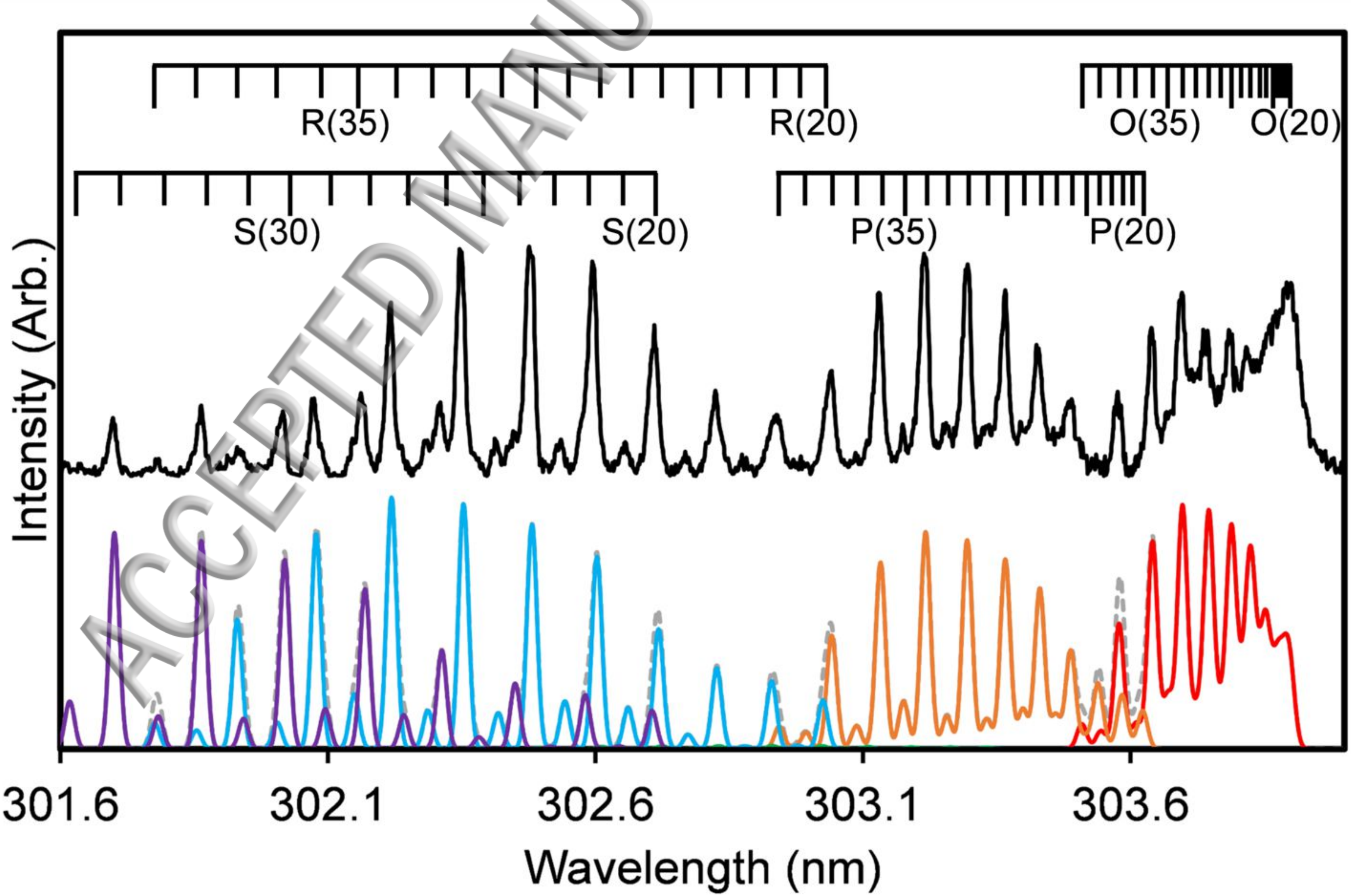
R(35)
R(20)
O(35)
O(20)
S(30)
S(20)
P(35)
P(20)
Intensity (Arb.)
301.6
302.1
302.6
303.1
303.6
Wavelength (nm)

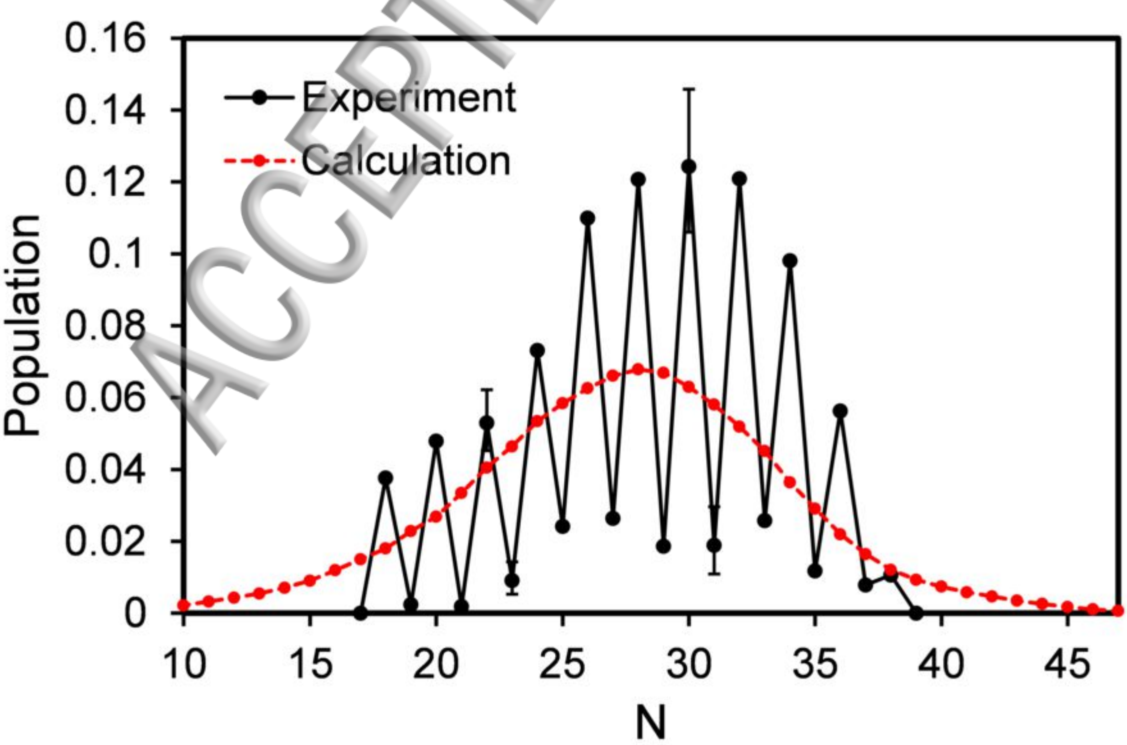
Experiment
Calculation
Population
0.16
0.14
0.12
0.1
0.08
0.06
0.04
0.02
0
10
15
20
25
30
35
40
45
N
ACCEPTED

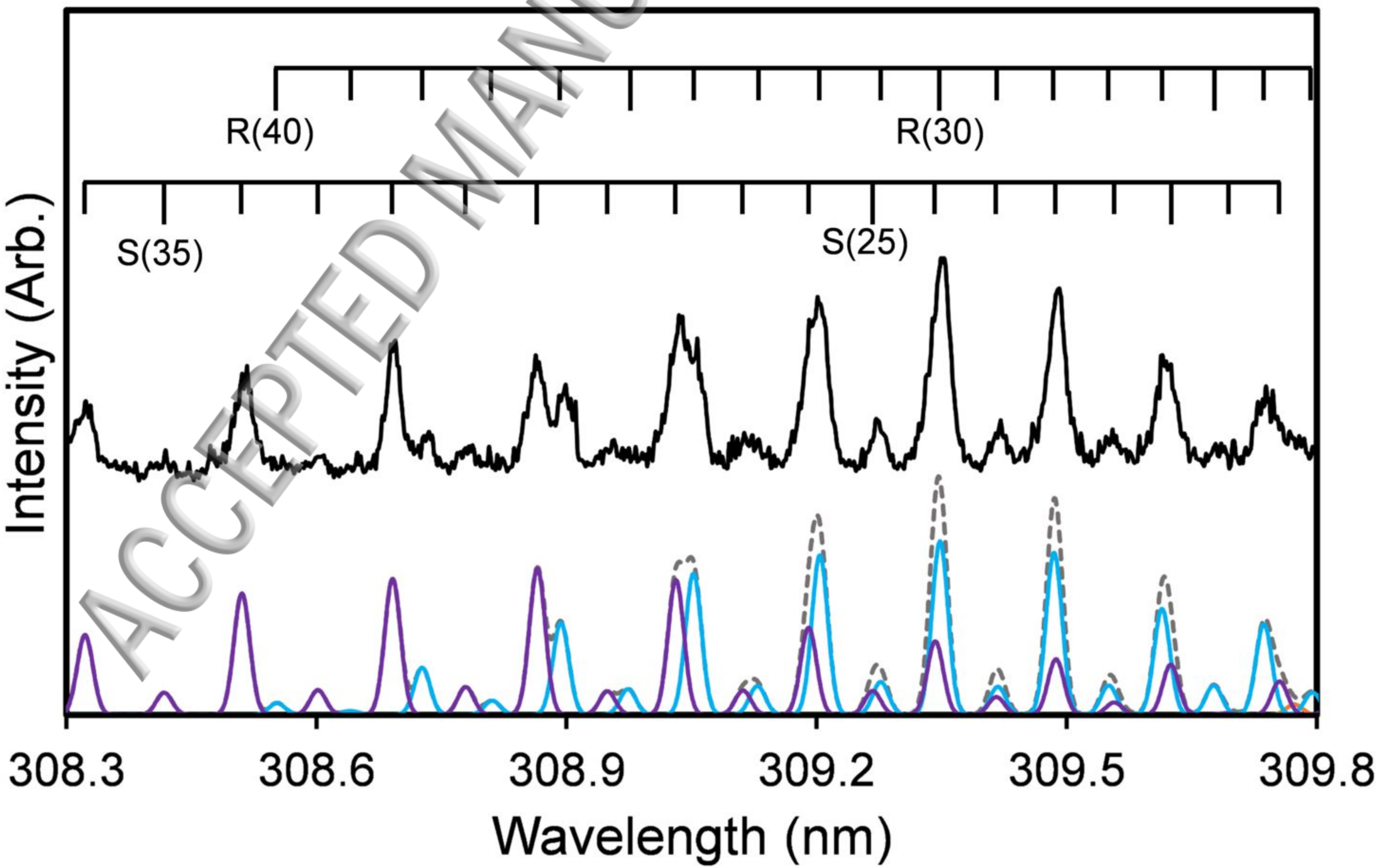
R(40)
R(30)
S(35)
S(25)
Intensity (Arb.)
308.3
308.6
308.9
309.2
309.5
309.8
Wavelength (nm)

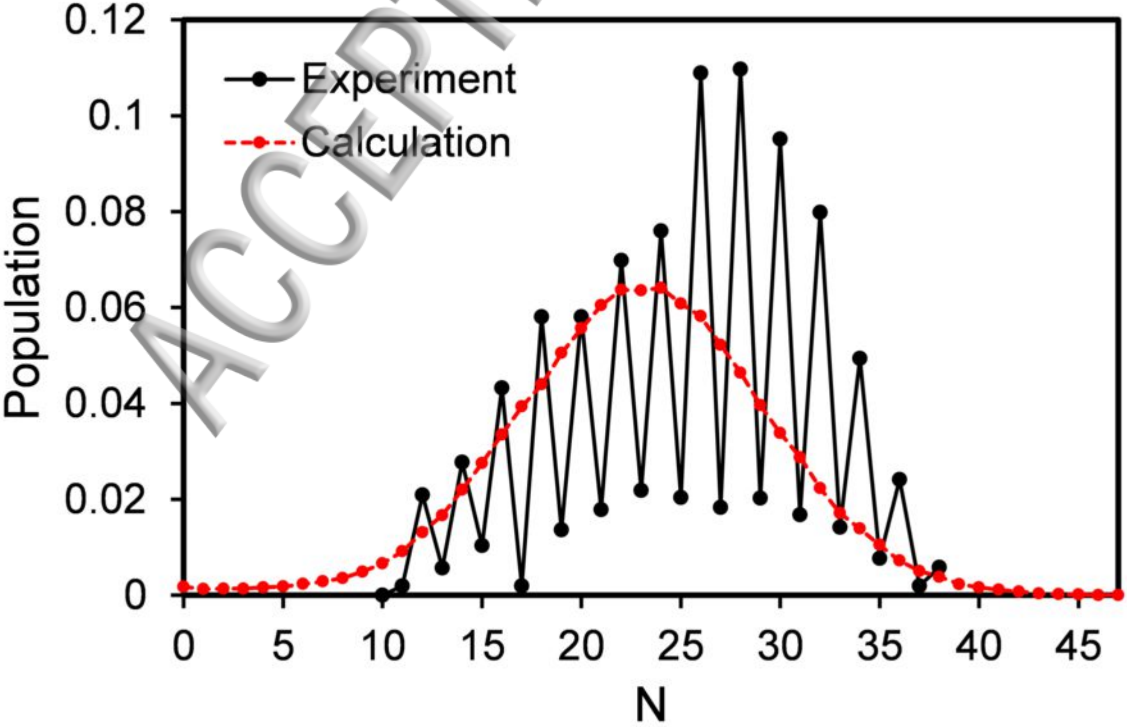

Experiment
Calculation
Population
N
0
0.02
0.04
0.06
0.08
0.1
0.12
0
5
10
15
20
25
30
35
40
45

ACCEPTED

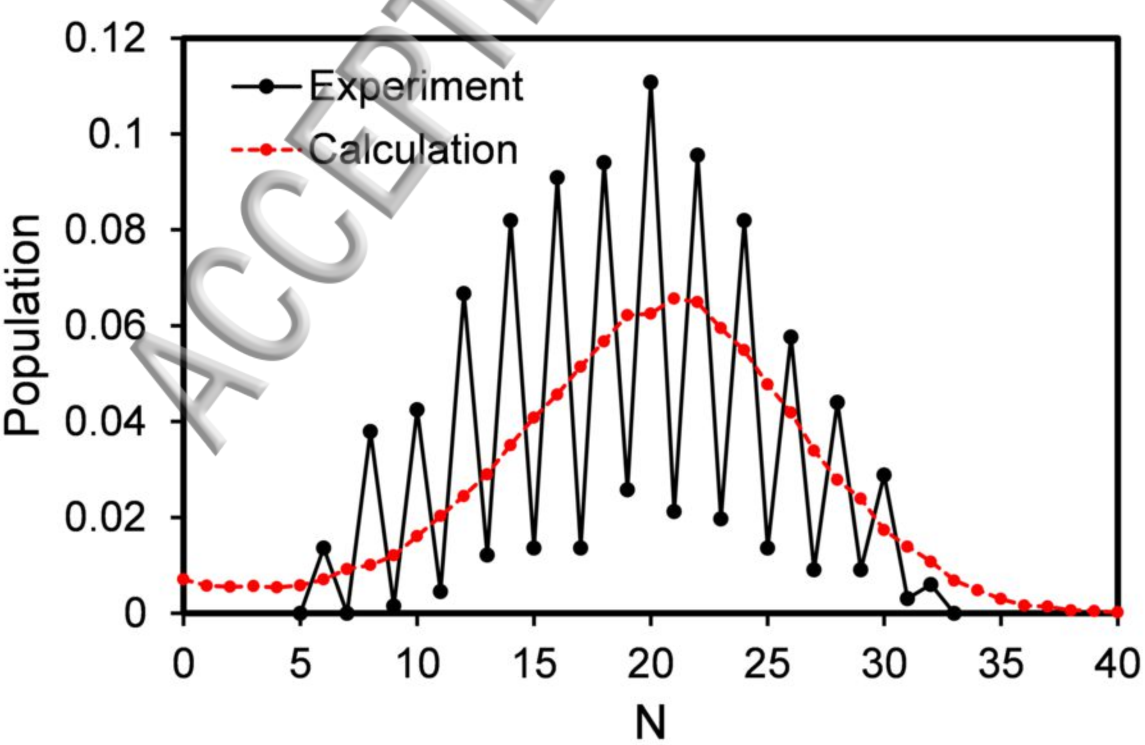
Experiment
Calculation
Population
N
0.12
0.1
0.08
0.06
0.04
0.02
0
0
5
10
15
20
25
30
35
40

ACCEPTED

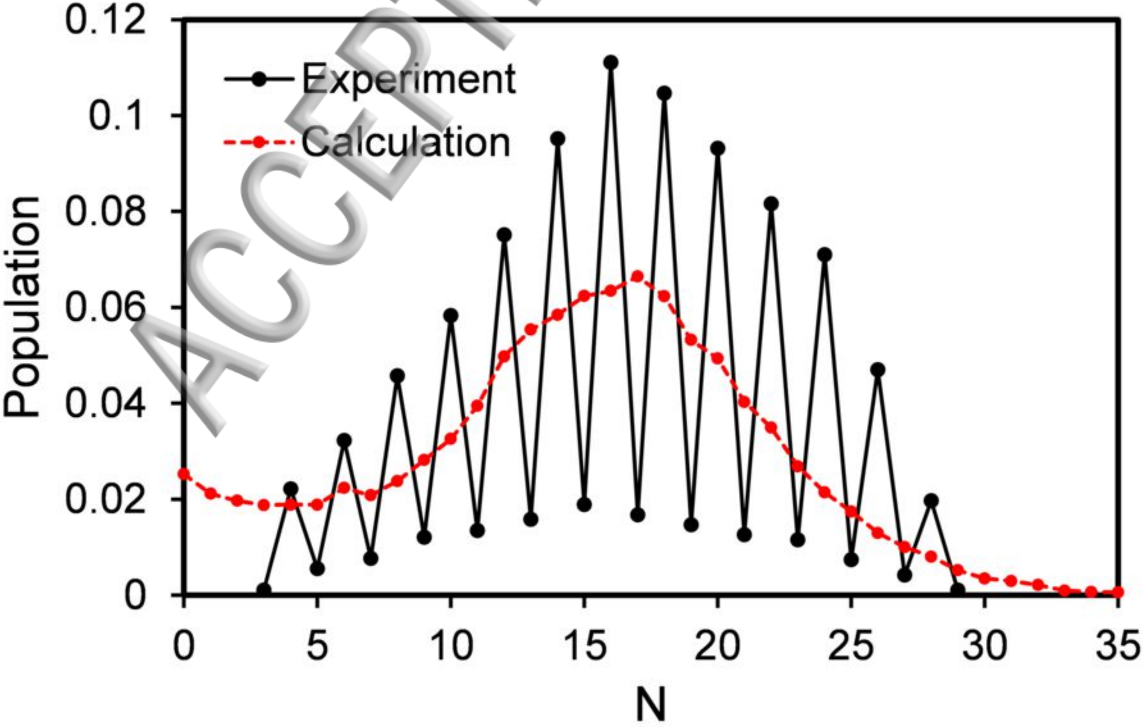

Population
N
0.12
0.1
0.08
0.06
0.04
0.02
0
0
5
10
15
20
25
30
35
Experiment
Calculation

ACCEPTED

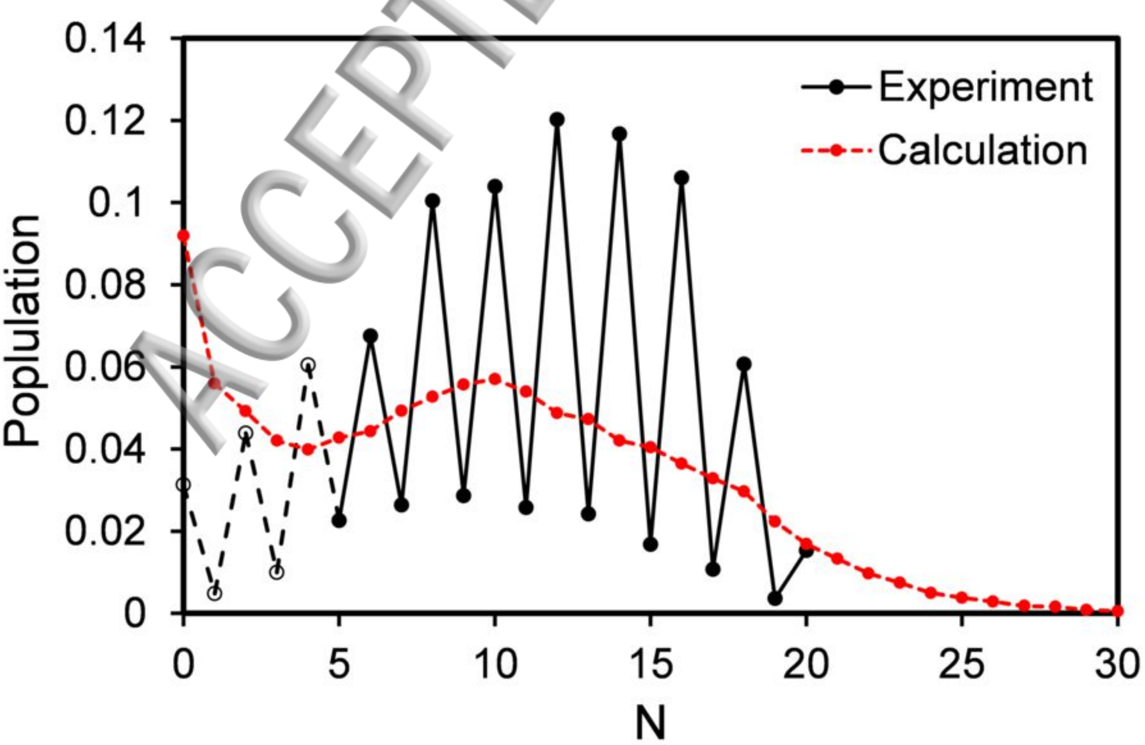

0.14
0.12
0.1
0.08
0.06
0.04
0.02
0
Poplulation
0
5
10
15
20
25
30
N
Experiment
Calculation

ACCEPTED

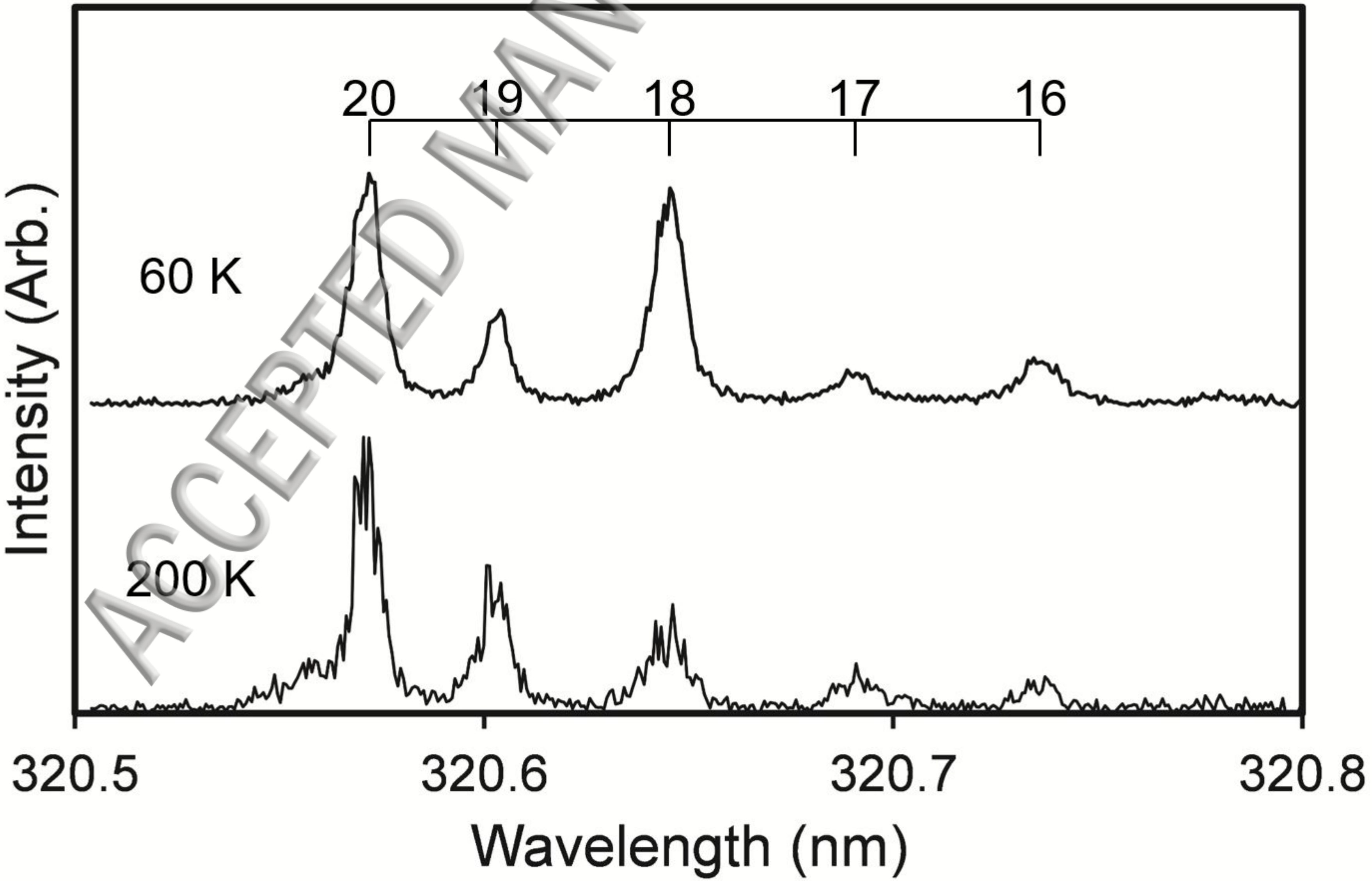
20
19
18
17
16
60 K
200 K
Intensity (Arb.)
320.5
320.6
320.7
320.8
Wavelength (nm)